Cross talk between Paneth and tuft cells drives dysbiosis and inflammation in the gut mucosa

Nathalie Coutry, Julie Nguyen, Salima Soualhi, François Gerbe, Victoria Meslier, Valérie Dardalhon, Mathieu Almeida, Benoit Quinquis, Florence Thirion, Fabien Herbert, et al.

PNAS

Main Manuscript for

Crosstalk between Paneth and tuft cells drives dysbiosis and inflammation in the gut mucosa

Nathalie Coutry[1,#,*], Julie Nguyen[1,#], Salima Soualhi[1,#], François Gerbe[1], Victoria Meslier[3], Valérie Dardalhon[2], Mathieu Almeida[3], Benoit Quinquis[3], Florence Thirion[3], Fabien Herbert[1], Imène Gasmi[1], Ali Lamrani[1], Alicia Giordano[1], Pierre Cesses[1], Laure Garnier[1], Steeve Thirard[1], Denis Greuet[1], Chantal Cazevieille[4], Florence Bernex[5], Christelle Bressuire[3,9], Douglas Winton[6], Ichiro Matsumoto[7], Hervé M. Blottière[3,8], Naomi Taylor[2] and Philippe Jay[1,*]

Affiliations

[1] Institute of Functional Genomics (IGF), University of Montpellier, CNRS, Inserm, Equipe Labellisée Ligue contre le Cancer, Montpellier, France

[2] Institut de Génétique Moléculaire de Montpellier, University of Montpellier, CNRS, Montpellier, France.

[3] Paris-Saclay University, INRAE, MetaGenoPolis, 78350 Jouy-en-Josas, France

[4] University of Montpellier, Institut des Neurosciences de Montpellier, France

[5] University of Montpellier, RHEM, BioCampus, CNRS, INSERM, Montpellier, France

[6] Cancer Research-UK Cambridge Institute, Li Ka Shing Centre, Robinson Way, Cambridge, CB2 0RE, UK.

[7] Monell Chemical Senses Center, 3500 Market Street, Philadelphia, Pennsylvania 19104, U.S.A.

[8] Nantes Université, INRAE, UR1280, PhAN, F-44000, Nantes, France

[9] Paris-Saclay University, INRAE, AgroParisTech, Micalis Institute, 78350 Jouy-en-Josas, France

[#] These authors contributed equally

[*] Corresponding authors: philippe.jay@igf.cnrs.fr, Nathalie.coutry@igf.cnrs.fr

Author Contributions: N.C., J.N. and S.S. performed the majority of the experiments. F.H., P.C., I.G., S.T., D.G., I.M., S.S., J.N. and D.W. contributed to mouse studies, V.M., M.A., F.T. and B.Q. performed shotgun metagenomic sequencing and analysis, S.S., F.B. and C.C. to characterization of the Sox9-deficient mouse line, A.G., L.G. and F.H. to organoid experiments, and V.D. to immune studies. P.J. conceived the study. P.J., N.C. designed experiments with contributions from F.G., V.D., and N.T. P.J. and N.C. wrote the manuscript with inputs from H.B., F.G. V.D. V.M. and N.T.

Competing Interest Statement: Authors declare no competing interests**.**

Classification: Biological Sciences/Cell Biology

Keywords: Microbiota dysbiosis, gut inflammation, tuft cells, Paneth cells, antimicrobial peptides

This PDF file includes:

Main Text
Figures 1 to 7
Tables 0

Abstract

Gut microbiota imbalance (dysbiosis) is increasingly associated with pathological conditions, both within and outside the gastrointestinal tract. Intestinal Paneth cells are considered to be guardians of the gut microbiota but the events linking Paneth cell dysfunction with dysbiosis remain unclear. We report a three-step mechanism for dysbiosis initiation. Initial alterations in Paneth cells, as frequently observed in obese and IBD patients, cause a mild remodeling of microbiota, with amplification of succinate-producing species. SucnR1-dependent activation of epithelial tuft cells triggers a type 2 immune response that, in turn, aggravates the Paneth cell defaults, promoting dysbiosis and chronic inflammation. We thus reveal a novel function of tuft cells in promoting dysbiosis following Paneth cell deficiency, and an unappreciated essential role of Paneth cells in maintaining a balanced microbiota to prevent inappropriate activation of tuft cells and deleterious dysbiosis. This succinate-tuft cell-inflammation circuit may also contribute to the chronic dysbiosis observed in patients.

Significance Statement

Dysbiosis underlies multiple diseases and can be caused by Paneth cell defects, as observed in obese or IBD patients. Since Paneth cells have microbe regulation properties, it is currently believed that their alterations directly cause dysbiosis. The main conceptual advance here is the demonstration that intestinal tuft cells play an essential role in establishing the dysbiosis, via a crosstalk with altered Paneth cells. We further identify bidirectional interactions between microbiota composition and the host inflammation status, which is controlled by tuft and Paneth epithelial cells. Our findings open perspectives for combinatorial therapies targeting both host and microbiota for a more effective management of dysbiosis-associated chronic diseases.

Main Text

Introduction

Alterations in the symbiosis between our organism and the gut microbiota constitute a critical parameter in the occurrence and severity of many diseases. The gut microbiota participates to the intestinal epithelial barrier and protection against pathogens by actively regulating multiple host physiological processes such as metabolism, circadian rhythmicity, digestion and immune responses (1). Importantly, the gut microbiota, which is established following delivery and breastfeeding, is highly dynamic. Throughout life, its composition varies with environmental and physiological factors such as nutrition, hormonal changes, lifestyle, and aging, amongst others (1). Perturbation of the microbiota composition and function, a state known as dysbiosis, impacts host homeostasis through altered host-microbiota interactions. Dysbiosis is notably associated with gastrointestinal tract diseases including inflammatory bowel diseases (IBD) and irritable bowel syndrome, as well as with extra gastrointestinal tract diseases ranging from metabolic syndrome, allergy and asthma, to psychiatric disorders (2–4). In many instances, dysbiosis not only accompanies the pathological state but is sufficient to recapitulate the pathology in previously healthy individuals, as demonstrated by microbiota transfer experiments in pre-clinical models (2, 5). Importantly, dysbiosis can be caused by both exogeneous factors such as high fat diet (6), or by endogenous changes, such as intestinal epithelial Paneth cell defects (7).

Epithelial Paneth cells were first identified as a critical component of the gut innate immunity involved in the defence against microorganisms (8, 9). Paneth cell differentiation depends on the Wnt signalling pathway (10) and one of its targets, the Sox9 transcription factor (11). Indeed, inactivation of *Sox9* in intestinal cells during mouse embryogenesis leads to the absence of Paneth cells and causes hyperplastic crypts with increased cell proliferation (12, 13). Interestingly, Paneth

cells are dysfunctional in Crohn's disease patients and in IBD murine models (14, 15); Paneth cell granules containing antimicrobial peptides display aberrant morphology and reduced secretion, and these alterations are linked to the establishment of dysbiosis (7). Paneth cell function is also altered in obese subjects, with reduced levels of antimicrobial peptides and features of ER stress (16), and rodents fed with a high fat diet display dysfunctional Paneth cells and associated dysbiosis (17). Deletion of genes encoding defensins (18) or lysozyme (19) further demonstrate the key role of Paneth cells as guardians of the gut microbiota integrity, with defective function serving as a driver of dysbiosis and inflammation. However, despite the tremendous impact of dysbiosis and inflammation on a multitude of diseases, the physiological mechanisms linking these processes to altered Paneth cell function remain to be investigated, to potentially provide new therapeutic opportunities to prevent or reverse dysbiosis.

Tuft cells have recently been revealed as key epithelial sentinels that initiate type 2 mucosal immunity following infections with parasites (20–22) or bacteria (23). Upon helminth infections, tuft cells respond by secreting the IL-25 alarmin cytokine, which in turn activates hematopoietic cells in the gut *lamina propria*, including type 2 innate lymphoid cells (ILC2). ILC2s produce type 2 cytokines, notably IL-13, which serve several functions, including remodeling of the intestinal epithelium with tuft and goblet cell hyperplasia, and eventual parasite expulsion. Mechanistically, tuft cell activation and immunomodulatory action, following parasite infection or artificial dysbiosis caused by polyethylene glycol (PEG) treatment, are dependent on the activation of several receptors including the SucnR1 succinate receptor (24–26), Tas2R taste receptors (27) and the olfactory receptor Vmn2r26 (23). Interestingly, mice with lysozyme-deficient Paneth cells exhibit an altered microbiota concomitant with a type 2 immune response including expansion of tuft cells (19). In addition, tuft cell numbers are strongly decreased in ileal lesions from Crohn's disease patients and in murine models of IBD (28), and an artificial increase in tuft cell numbers in genetically engineered IBD mouse models improves their inflammatory status (28). Altogether, these results suggest potential cooperation of Paneth and tuft cells to regulate gut microbiota homeostasis and dysbiosis as well as the status of gut mucosa inflammation.

Here, we investigated the hypothesis that a crosstalk between Paneth cells and tuft cells drives dysbiosis initiation. Using a murine model with dysfunctional Paneth cells, we show that dysbiosis develops, resulting in a type 2-dominated gut inflammation. Importantly, we found that a crosstalk between Paneth cells and chemosensory tuft cells is required to establish dysbiosis. The absence of tuft cells causes a dramatic reduction in inflammation and dysbiosis, even in the context of Paneth cell defects. Mechanistically, we identify a critical role for the SucnR1 tuft cell receptor to link Paneth cell defects with tuft cell activation, a process that occurs independently of the Trpm5 signalling pathway. We thus describe a novel "Paneth cell-succinate-tuft cell-immune system"

circuit that drives dysbiosis, with relevance for inflammatory bowel diseases and other conditions involving altered Paneth cells.

Results

Maintenance of intestinal Paneth cell function requires the Sox9 transcription factor

Deletion of the Paneth cell transcription factor Sox9 (11) in the intestinal epithelium during embryonic development (*Sox9$^{LoxP/LoxP}$;Villin-Cre*) causes a complete absence of Paneth cells as assessed by expression of lysozyme, a Paneth cell marker (12, 13). We first examined the consequences of *Sox9* deletion, induced in the adult intestinal epithelium, on Paneth cell generation. In adult *Sox9$^{LoxP/LoxP}$;Villin-Cre^{ERT2}* mice, the Sox9 protein became undetectable as early as 3 days after tamoxifen treatment (Figure S1a). However, lysozyme-expressing epithelial cells were still detectable at the base of intestinal crypts 2 weeks after tamoxifen treatment (Figure 1a). Since the life span of adult mouse Paneth cells is approximately 2 months (29), most of these lysozyme-expressing cells were present prior to *Sox9* deletion, indicating that Sox9 is not required for the survival of previously differentiated Paneth cells. In addition, lysozyme-expressing Paneth cells were still present several months after *Sox9* deletion (Figure S1a). BrdU incorporation studies were performed to determine whether these cells were able to differentiate from *Sox9*-deleted stem/precursor cells. Equivalent percentages of BrdU$^+$/lysozyme$^+$ Paneth cells were detected in *Sox9*-deficient mice and their littermate controls, accounting for approximately 35% of all Paneth cells after 3 weeks of BrdU treatment. Thus, new Paneth cells were generated at similar rates in both mice genotypes (Figure S1b). However, there was a significantly higher proportion of mislocalized Paneth cells in the upper crypt and villus compartments in *Sox9*-deficient mice (15%) as compared to littermate controls (2%), likely explaining the lower number of Paneth cells at the crypt base in the *Sox9*-deficient mice (Figure S1c and S1d).

Cellular morphology of *Sox9*-deficient Paneth cells was also altered; lysozyme-containing secretion granules were more diffuse and heterogenous in *Sox9*-deficient as compared to wild type Paneth cells (Figure 1b). In line with these data, electron microscopy analyses from 3 days to 4 months following *Sox9* deletion revealed a dramatically reduced size of electron-dense secretory granules, embedded within an electron-lucent structure suggestive of mucus, a substance not normally produced by Paneth cells (Figure 1c). Importantly, these alterations in secretion granule morphology were not detected in *Sox9$^{LoxP/LoxP}$;P450a1-Cre* mice (Figure 1b and 1c), in which genetic recombination occurs in all intestinal epithelial cells except Paneth cells (29), one week following treatment with β-naphtoflavone. However, as expected, a proportion of Paneth cells from *Sox9$^{LoxP/LoxP}$;P450a1-Cre* mice also displayed abnormal granules one month after *Sox9* deletion (Figure S1e), due to Paneth cell population turnover and replacement by new, altered, Paneth cells

generated from *Sox9*-deleted epithelial stem cells. These data indicate that maintenance of mature Paneth cells requires *Sox9* in a cell-autonomous manner (Figure 1b).

As intestinal goblet cells express Muc2, the main constituent of small intestinal mucus, and their differentiation requires the Klf4 transcription factor (30), we next assessed whether *Sox9*-deficient Paneth cells harbour an intermediate phenotype with mixed features of Paneth and goblet cells (31). Indeed, *Sox9*-deficient Paneth cells expressed significant levels of Muc2 and Klf4, which were not detected in normal Paneth cells from control mice (Figure 1d, Figure S1f). Moreover, since Paneth cell granules contain anti-microbial peptides, we hypothesized that their altered morphology in *Sox9*-deficient mice would be associated with altered production of these peptides. Indeed, the presence of altered Paneth cells in *Sox9$^{LoxP/LoxP}$;Villin-Cre^{ERT2}* mice was associated with a strongly decreased expression of critical antimicrobial peptides such as lysozyme, defensin α29, Reg3β and Reg3γ, as well as the Mmp7 matrix metallopeptidase, which is involved in the activation of defensins (32) (Figure 1e).

Thus, Sox9 deletion in adult mice does not impact the survival of Paneth cells nor their early differentiation. Notably though, *Sox9*-deficient Paneth cells have a strongly modified phenotype, as shown by the altered morphology of lysozyme$^+$ secretion granules as well as Muc2 and Klf4 expression, and moreover, they are frequently mislocalized throughout the crypt and villus compartments. *Sox9$^{LoxP/LoxP}$;Villin-Cre^{ERT2}* mice therefore constitute a novel model to study the consequences of Paneth cell alterations in adult intestinal physiopathology.

Abnormal Paneth cells are associated with intestinal dysbiosis and disruption of the intestinal mucosal barrier

An unbalanced microbiota and defects in intestinal permeability are frequent features of gut diseases. As antimicrobial peptides are essential effectors of host-microbiota interactions (33) and their levels are strongly reduced in *Sox9$^{LoxP/LoxP}$;Villin-Cre^{ERT2}* mice, we next evaluated whether the presence of *Sox9*-deficient Paneth cells results in impaired microbiota regulation. Bacterial 16S profiling of faeces from *Sox9$^{LoxP/LoxP}$;Villin-Cre^{ERT2}* mice and *Sox9$^{LoxP/LoxP}$* control mice revealed a significant shift in intestinal microbial populations one month following *Sox9* deletion. While the global bacterial load was unaffected, the beta diversity of microbial communities differed significantly between *Sox9$^{LoxP/LoxP}$* and *Sox9$^{LoxP/LoxP}$;Villin-Cre^{ERT2}* mice (Figure 2a).

We then investigated intestinal epithelial permeability in control and *Sox9$^{LoxP/LoxP}$;Villin-Cre^{ERT2}* mice. After gavage with FITC-dextran, *Sox9$^{LoxP/LoxP}$;Villin-Cre^{ERT2}* mice exhibited a significantly increased translocation of FITC-dextran from the gastrointestinal tract into the circulation as

compared to littermate *Sox9*$^{LoxP/LoxP}$ controls. In contrast, no increase in epithelial permeability was observed in *Sox9*$^{LoxP/LoxP}$*;P450a1-Cre* mice, indicating that *Sox9* deletion in Paneth cells, but not in other epithelial cell lineages, underlies increased paracellular permeability in *Sox9*$^{LoxP/LoxP}$*;Villin-Cre*^{ERT2} mice (Figure 2b). Together, these results strongly suggest that altered Paneth cell morphology and antimicrobial peptides production hamper their function, causing an imbalance in the microbiota, and a disruption of intestinal barrier integrity.

Changes in mucosal immunity due to dysfunctional Paneth cells is dependent on IL-4/IL-13 signalling and presence of a microbiota

The intestinal dysbiosis-linked increase in epithelial permeability facilitates access of microbes and their products to *lamina propria* immune cells, and downstream inflammation (34–36). We therefore sought to determine the inflammatory state in control and *Sox9*$^{LoxP/LoxP}$*;Villin-Cre*^{ERT2} mice. To assess whether altered Paneth cell function and impaired microbiota regulation were associated with changes in intestinal immunity, we profiled expression of key components of type 1 (*Tbx21, Ifn*γ*, Tnf*α), type 2 (*Gata3, Il4, Il13, Il25, Il33*), and type 17 (*Rorc, Il17a, Il21, Il22*) immune responses. Comparisons of control *Sox9*$^{LoxP/LoxP}$ mice and *Sox9*$^{LoxP/LoxP}$*;Villin-Cre*^{ERT2} mice revealed significant increases in several components of type 2 immune responses including expression of *Il4*, *Il13* and *Il25* cytokine genes in the latter mice. In contrast, expression of genes associated with type 1 and type 17 responses were not elevated in *Sox9*$^{LoxP/LoxP}$*;Villin-Cre*^{ERT2} mice, with significant decreases in *Tnf*, *Rorc* and *Il22* genes (Figure 3a). These data suggest unbalanced immune cell populations in mice with *Sox9*-deficient Paneth cells, with a shift towards type 2 immune cell populations.

A detailed immunohistochemical analysis of the *lamina propria* of *Sox9*$^{LoxP/LoxP}$*;Villin-Cre*^{ERT2} mice revealed higher densities of major basic protein (MBP)-expressing eosinophils and Gata3^{+} immune cells (Figure 3b and 3c). The Gata3 transcription factor is involved in the differentiation of both CD3^{+} Th2 lymphocytes and CD3^{-} type 2 innate lymphoid cells (37). Co-staining of Gata3 and CD3, used to discriminate Th2 and ILC2 subsets (20), demonstrated a predominantly increased ILC2 population in the *lamina* propria of *Sox9*$^{LoxP/LoxP}$*;Villin-Cre*^{ERT2} mice as compared to *Sox9*$^{LoxP/LoxP}$ mice ($p<0.0001$), with an unchanged Th2 population (Figure S2a and S2b). Thus, the presence of altered Paneth cell function is linked to the presence of a type 2 dominated inflammation, concomitant with an increased population of Gata3^{+}CD3^{-} immune cells, likely representing ILC2s.

The epithelial compartment also displayed features of a type 2 immune response (20), with significant increases in Dclk1^{+} tuft cells and PAS-stained goblet cells (Figure 3d and 3e). Moreover,

expression of the Resistin-like beta peptide (Retnlβ), an immune effector peptide produced by small intestinal goblet cells during type 2 immune responses (38), was detected in mice with *Sox9*-deleted Paneth cells but not in control mice (Figure 3d and 3e). Paneth cell dysfunction was central to these type 2 immune response features as they were not present in *Sox9$^{LoxP/LoxP}$;P450a1-Cre* mice (Figure S2c). To investigate the link between altered Paneth cells and the type 2 inflammation observed in *Sox9$^{LoxP/LoxP}$;Villin-Cre^{ERT2}* mice, we crossed these mice with *Il-4Rα*-deficient mice, in which both the IL-4 and IL-13 dimeric receptors are non-functional (39). In *Sox9$^{LoxP/LoxP}$;Villin-Cre^{ERT2};Il-4Rα$^{-/-}$* mice, a type 2 response was initiated, as shown by the significantly higher number of Gata3^{+} cells in the *lamina propria* as compared to *Sox9*-control mice (Figure S2d; $p<0.0001$ and S2e). However, in the absence of IL-4/IL-13 signalling-mediated epithelial remodelling, the *Sox9$^{LoxP/LoxP}$;Villin-Cre^{ERT2};Il-4Rα$^{-/-}$* mice did not exhibit hyperplasia of Dclk1^{+} tuft cells nor goblet cells (Alcian blue staining). Furthermore, Retnlβ expression by goblet cells was not detected (Figure S2d) and epithelial paracellular permeability was not elevated in *Sox9$^{LoxP/LoxP}$;Villin-Cre^{ERT2};Il-4Rα$^{-/-}$* mice (Figure S2f). Thus, the decreased antimicrobial control, dysbiosis, increased trans-epithelial permeability, and type 2 inflammation observed in mice with *Sox9*-deficent Paneth cells are dependent on an intact IL-4/IL-13 signalling axis.

We next investigated whether the link between altered Paneth cells and trans-epithelial permeability and inflammation was directly dependent on the microbiota. Wide spectrum antibiotic treatment concomitant with *Sox9* deletion did not change the differentiation of altered Paneth cells in *Sox9$^{LoxP/LoxP}$;Villin-Cre^{ERT2}* mice; they maintained small and diffuse secretion granules and exhibited Muc2 and Klf4 expression (Figure S3a and S3b). However, in sharp contrast with the increased trans-epithelial permeability observed in non-antibiotic-treated *Sox9$^{LoxP/LoxP}$;Villin-Cre^{ERT2}* mice (Figure 2b), permeability was not elevated in antibiotic-treated *Sox9$^{LoxP/LoxP}$;Villin-Cre^{ERT2}* mice as compared to *Sox9$^{LoxP/LoxP}$* mice (Figure S3c). Furthermore, no evidence of type 2 inflammation was found in antibiotic-treated *Sox9$^{LoxP/LoxP}$;Villin-Cre^{ERT2}* mice, with tuft cell, goblet cell, MBP^{+} eosinophil, Gata3^{+} Th2 and ILC2 cell numbers, as well as Retnlβ expression indiscernible from those detected in *Sox9$^{LoxP/LoxP}$* control animals (Figure S3d and Se). These data establish the microbiota milieu as a required link in the altered epithelial permeability and inflammation caused by abnormal Paneth cells.

Tuft cells mediate the effects of altered Paneth cells on type 2 inflammation and trans-epithelial permeability

In addition to the microbiota milieu, we and others have shown that intestinal epithelial tuft cells play an integral part in the initiation of a type 2 immune response in response to the presence of parasites in the gut lumen by secreting the IL-25 alarmin cytokine (20, 22, 21). However, the role

of tuft cells in initiating responses in the context of a physiological dysbiosis remain unknown. To evaluate whether intestinal tuft cells are involved in the Paneth cell-dysbiosis-type 2 inflammation axis, tuft cells were eliminated by knockout of the Pou2f3 transcription factor (20). Specifically, *Sox9*$^{LoxP/LoxP}$*;Villin-Cre*^{ERT2} mice were crossed with the *Pou2f3*$^{-/-}$ line to generate *Sox9*$^{LoxP/LoxP}$*;Villin-Cre*^{ERT2};*Pou2f3*$^{-/-}$ compound mice. Following *Sox9* deletion in *Sox9*$^{LoxP/LoxP}$*;Villin-Cre*^{ERT2};*Pou2f3*$^{-/-}$ compound mice, Paneth cells displayed the same abnormal morphology that was detected in *Sox9*$^{LoxP/LoxP}$*;Villin-Cre*^{ERT2} mice with diffuse lysozyme staining as well as Muc2 and Klf4 expression (Figure 4a and Figure S4a). Strikingly, though, *Sox9*$^{LoxP/LoxP}$*;Villin-Cre*^{ERT2};*Pou2f3*$^{-/-}$ mice exhibited no increase in trans-epithelial permeability (Figure 4b) and their type 2 inflammation parameters were indiscernible from those of *Sox9*$^{LoxP/LoxP}$ control mice (Figure 4c and Figure S4b). These data reveal a new and essential role for tuft cells in linking the dysbiosis resulting from altered Paneth cells with the induction of a type 2 inflammatory response. Thus, our data identify a novel Paneth cell-microbiota-tuft cell-immune system circuit that regulates gut homeostasis.

A Paneth-tuft cell crosstalk underlies the dysbiosis occurring following Paneth cell dysfunction

To further investigate the impact of tuft cells on the gut microbial populations in the context of Paneth cell deficiency, we performed shotgun metagenomic sequencing on caecum samples from *Sox9*$^{LoxP/LoxP}$, *Sox9*$^{LoxP/LoxP}$*;Villin-Cre*^{ERT2}, *Pou2f3*$^{-/-}$ and *Sox9*$^{LoxP/LoxP}$*;Villin-Cre*^{ERT2};*Pou2f3*$^{-/-}$ mice. As the caecum microbiota is more relevant to the ileum microbiota than the fecal one, we focused on caecum samples. Bacterial gene richness, which reflects diversity of microbiota bacterial species, was significantly decreased in *Sox9*$^{LoxP/LoxP}$*;Villin-Cre*^{ERT2} mice as compared to control *Sox9*$^{LoxP/LoxP}$ mice ($p=0.007$), thus confirming our previous 16S analyses (Figure 2a). Furthermore, no significant differences were observed between *Pou2f3*$^{-/-}$ mice as compared to *Sox9*$^{LoxP/LoxP}$ control mice ($p>0.05$). Importantly though, gene richness remained high in *Sox9*$^{LoxP/LoxP}$*;Villin-Cre*^{ERT2};*Pou2f3*$^{-/-}$ mice that have altered Paneth cells in the absence of tuft cells, at levels comparable to those detected in *Sox9*$^{LoxP/LoxP}$ mice (Figure 5a).

Differential abundance analyses of Metagenomic Species Pangenome (MSP) microbial species between the different mouse groups followed the same trend. After adjustment for multiple testing and using a q-value threshold of 0.05, 40 MSP microbial species were identified as exhibiting differential abundance between *Sox9*$^{LoxP/LoxP}$ and *Sox9*$^{LoxP/LoxP}$*;Villin-Cre*^{ERT2} mice. While some of the differentially represented MSP microbial species could not be taxonomically assigned at the species level, we detected an enrichment of MSP microbial species of the *Bacteroidales* order in *Sox9*$^{LoxP/LoxP}$*;Villin-Cre*^{ERT2} mice, while MSP microbial species belonging to the *Clostridiales* order

were preferentially enriched in *Sox9*$^{LoxP/LoxP}$ mice (Figure S5a). Marked alterations in the caecum microbiota were also found upon comparison of *Sox9*$^{LoxP/LoxP}$*;Villin-Cre*^{ERT2} and *Sox9*$^{LoxP/LoxP}$*;Villin-Cre*^{ERT2};*Pou2f3*$^{-/-}$ mice, with 57 differentially abundant MSP species (q-value<0.05); there was a similar trend of enrichment of members of the *Bacteroidales* in the *Sox9*$^{LoxP/LoxP}$*;Villin-Cre*^{ERT2} group (Figure S5b). No differences were detected between *Sox9*$^{LoxP/LoxP}$ and *Pou2f3*$^{-/-}$ mice, nor between wild type and *Sox9*$^{LoxP/LoxP}$*;Villin-Cre*^{ERT2};*Pou2f3*$^{-/-}$ mice, as assessed by the q-value threshold. Taken together, these data indicate that microbiota alterations caused by Paneth cell alterations are markedly reduced in the absence of tuft cells and downstream type 2 inflammation. Thus, tuft cell-dependent type 2 inflammation enhances the initial effects of Paneth cell dysfunction to promote dysbiosis.

Tuft cell activation relies on a Trpm5-independent induction of the Succinate-SucnR1 axis

Our results demonstrate that dysbiosis establishment requires a crosstalk between Paneth and tuft cells. We were therefore interested in identifying the molecular mechanism underlying this crosstalk, and specifically, to understand how the remodelled microbiota, caused by abnormal Paneth cells, activates tuft cells. Metagenomic quantitative analysis of microbiota revealed an enrichment of MSP microbial species of the *Bacteroidales* order in *Sox9*$^{LoxP/LoxP}$*;Villin-Cre*^{ERT2} mice as compared to *Sox9*$^{LoxP/LoxP}$ mice (Figure S5a and b). Furthermore, analyses of differentially abundant gut metabolic modules (GMM) between *Sox9*$^{LoxP/LoxP}$*;Villin-Cre*^{ERT2} and *Sox9*$^{LoxP/LoxP}$ mice revealed 30 GMM enriched in the *Sox9*$^{LoxP/LoxP}$*;Villin-Cre*^{ERT2} mice with a q-value <0.05 (Table S1). Among the metabolic pathways enriched in *Sox9*$^{LoxP/LoxP}$*;Villin-Cre*^{ERT2} mice as compared to *Sox9*$^{LoxP/LoxP}$ mice, succinate production (p-value<0.001; q-value<0.005) drew our attention. Indeed, succinate produced by parasites has the potential to activate tuft cells via SucnR1, specifically expressed on tuft cells among intestinal epithelial cells (25, 26), thus constituting an attractive candidate to link dysbiosis with tuft cell activation. Succinate-SucnR1 signalling triggers a type 2 immune response (25, 26) which can also be recapitulated by treating mice with polyethylene glycol and streptomycin, described to increase succinate-producing microbiota (24). Importantly, bacteria from the *Bacteroidales* order, which includes the *Prevotella* genus, were enriched in our metagenomic analyses (Figure S5a), and produce succinate (40). To investigate the potential role of succinate, we first assessed the potential for succinate production of MSP microbial species with differential representation in *Sox9*$^{LoxP/LoxP}$ and *Sox9*$^{LoxP/LoxP}$*;Villin-Cre*^{ERT2} mice (Figure S5a) by a quantitative analysis of the genes involved in the two final steps performed under anaerobic conditions (Malate->Fumarate, Fumarate->Succinate) (Figure 5b and Supporting information). Global completeness of the final steps for succinate production, i.e. the proportion of

detected Kegg Orthologues (KOs) that are necessary to produce succinate in each microbial species, was significantly higher in the MSP species enriched in *Sox9$^{LoxP/LoxP}$;Villin-Cre^{ERT2}* mice (mean ± sd = 39% ± 24%), as compared to the MSP species enriched in *Sox9$^{LoxP/LoxP}$* mice (mean ± sd = 22% ± 20%; p = 0.017; Figure 5c). Thus, microbiota from *Sox9$^{LoxP/LoxP}$;Villin-Cre^{ERT2}* mice exhibit a higher functional potential for succinate production as compared to that of control mice.

To determine whether succinate plays a functional role in activating tuft cells in mice with *Sox9*-deficient Paneth cells, we generated compound *Sox9$^{LoxP/LoxP}$;Villin-Cre^{ERT2};SucnR1$^{-/-}$* mice. Notably, both trans-epithelial permeability and markers of type 2 immunity were low in *Sox9$^{LoxP/LoxP}$;SucnR1$^{+/+}$*, *Sox9$^{LoxP/LoxP}$;SucnR1$^{-/-}$* and *Sox9$^{LoxP/LoxP}$;Villin-Cre^{ERT2};SucnR1$^{-/-}$* mice, as compared to *Sox9$^{LoxP/LoxP}$;Villin-Cre^{ERT2}* mice (Figure 5d and 5e). These data demonstrate the essential role of SucnR1 signalling in the initiation of tuft cell-dependent type 2 inflammation, even in the context of Paneth cell alterations with decreased *lysozyme*, *Mmp7* and *Defa29* expression, and concomitant microbiota changes.

In addition to the importance of SucnR1 in tuft cell activation, several studies have reported a critical role of the transient receptor potential cation channel, subfamily M, member 5 (Trpm5) in mediating tuft cell responses (21, 24, 26, 27). To explore the potential involvement of Trpm5 in tuft cell activation in the context of abnormal Paneth cells, we generated compound *Sox9$^{LoxP/LoxP}$;Villin-Cre^{ERT2};Trpm5$^{-/-}$* mice. While *Sox9$^{LoxP/LoxP}$;Trpm5$^{-/-}$* mice did not exhibit elevated trans-epithelial permeability or expression of type 2 inflammation markers, these parameters were markedly increased in *Sox9$^{LoxP/LoxP}$;Villin-Cre^{ERT2};Trpm5$^{-/-}$* mice, at levels equivalent to those detected in *Sox9$^{LoxP/LoxP}$;Villin-Cre^{ERT2};Trpm5$^{+/+}$* mice (Figure S6a andS6b). Thus, tuft cell-dependent type 2 inflammation in response to dysfunctional Paneth cells is mediated by SucnR1 *via* a Trpm5-independent pathway.

Tuft cell-mediated type 2 immunity downregulates expression of antimicrobial RegIII in Paneth cells

To more precisely study the mechanisms *via* which tuft cell-dependent type 2 inflammation mediates dysbiosis in the context of dysfunctional Paneth cells, we first assessed the consequences of *Sox9* deletion in organoids derived from *Sox9$^{LoxP/LoxP}$;Villin-Cre^{ERT2}* and *Sox9$^{LoxP/LoxP}$* control mice. In this *ex vivo* epithelium culture system, the absence of immune cells, microbiota and other non-epithelial cells, allows the direct consequences of altered Paneth cells to be distinguished from the effects due to inflammation. Treatment with 4-OH-tamoxifen rapidly and efficiently caused *Sox9* deletion in *Sox9$^{LoxP/LoxP}$;Villin-Cre^{ERT2}* organoids but not in *Sox9$^{LoxP/LoxP}$*

controls (Figure S7a). 5 days after 4-OH-tamoxifen treatment, Paneth cell morphology was altered in *Sox9*-deficient organoids, with decreased granule size as compared to control *Sox9*$^{LoxP/LoxP}$ organoids as well as abnormal expression of Klf4 in Paneth cells (Figure S7a). Furthermore, analysis of Paneth cell markers revealed strongly reduced lysozyme, matrix metallopeptidase-7 (Mmp7) and defensin alpha 29 (Defa29) expression in *Sox9*$^{LoxP/LoxP}$*;Villin-Cre*^{ERT2} organoids as compared to *Sox9*$^{LoxP/LoxP}$ controls (Figure 6a), in accord with our *in vivo* data (Figure 1e). Notably though, in sharp contrast with *in vivo* data in *Sox9*$^{LoxP/LoxP}$*;Villin-Cre*^{ERT2} mice, expression of *regenerating islet-derived 3-beta* (*RegIII*β) and *–gamma* (*RegIII*γ) were not altered in *Sox9*$^{LoxP/LoxP}$*;Villin-Cre*^{ERT2} organoids (Figure 6a). RegIIIβ and RegIIIγ belong to the family of C-type lectins, which have direct bactericidal properties by binding the cell wall of gram-positive bacteria (41). These data thus suggest that the attenuated *RegIII*β and *RegIII*γ expression observed in Paneth cells in *Sox9*$^{LoxP/LoxP}$*;Villin-Cre*^{ERT2} mice is a consequence of the type 2 inflammation caused by the Paneth cell-tuft cell crosstalk -and not to Paneth cells alone- promoting dysbiosis in these mice.

We then evaluated the potential of IL-13, a key cytokine produced in the context of type 2 immune responses (42), to induce the downregulation of RegIII expression in cultured organoids. *Sox9* was deleted as above, and half of the organoids were then treated with recombinant IL-13 (rIL-13) during 72 hours before analysis. As we previously showed (Figure 6a), *Sox9* deletion in organoids did not affect significantly *RegIII*β and *RegIII*γ gene expression. Notably, exposure to rIL-13 increased expression of the *Pou2f3* tuft cell maker and *Retnl*β in goblet cells, indicating efficient epithelial remodelling, and significantly reduced expression of *RegIII*β and *RegIII*γ (Figure S7b). Thus, in the context of *Sox9* deficiency, the presence of a single type 2 cytokine is sufficient to downregulate RegIII in Paneth cells.

In a reciprocal experiment, aimed at evaluating the importance of the inflammatory environment in the reduced *RegIII*β and *RegIII*γ expression in mice with altered Paneth cells, we used *Sox9*$^{LoxP/LoxP}$*;Villin-Cre*^{ERT2};*Pou2f3*$^{-/-}$ mice as a model for Paneth cell dysfunction in the absence of type 2 inflammation. Interestingly, *lysozyme*, *Mmp7* and *Defa29* expression were strongly reduced in both *Sox9*$^{LoxP/LoxP}$*;Villin-Cre*^{ERT2} and *Sox9*$^{LoxP/LoxP}$*;Villin-Cre*^{ERT2};*Pou2f3*$^{-/-}$ models as compared to control mice, identifying these genes as epithelial cell intrinsic consequences of *Sox9* deletion in Paneth cells. In sharp contrast, expression of *RegIII*β and *RegIII*γ remained high in *Sox9*$^{LoxP/LoxP}$*;Villin-Cre*^{ERT2};*Pou2f3*$^{-/-}$ mice (Figure 6b), characterized by the absence of type 2 inflammation and an absence of dysbiosis. Indeed, *RegIII*β and *RegIII*γ levels were significantly higher than those detected in *Sox9*$^{LoxP/LoxP}$*;Villin-Cre*^{ERT2} mice, with an established dysbiosis and active type 2 inflammation (Figure 6b). Interestingly, similar results were observed in

Sox9$^{LoxP/LoxP}$*;Villin-Cre*^{ERT2};*Il-4Rα*$^{-/-}$ mice, where *RegIIIβ* and *RegIIIγ* levels were similar to those detected in *Sox9*$^{LoxP/LoxP}$*;Il-4Rα*$^{+/+}$ mice (Figure S7c). Thus, the loss of *RegIIIβ* and *RegIIIγ* in epithelial cells is dependent on the inflammatory milieu, especially on the type 2 cytokine IL13, and this change likely contributes to the emergence of intestinal dysbiosis of *Sox9*$^{LoxP/LoxP}$*;Villin-Cre*^{ERT2} mice.

Altogether, these data support the hypothesis of a step-wise model of dysbiosis in the context of abnormal Paneth cells: 1- dysfunctional Paneth cells first induce mild changes in microbiota composition which activate tuft cells; 2- tuft cell activation then triggers gut inflammation; and 3- the inflammatory environment promotes further microbiota remodelling via *RegIIIβ* and *RegIIIγ* down-regulation in epithelial cells, eventually leading to dysbiosis.

To test this hypothesis, we performed a kinetic analysis of the main epithelial and immune system parameters occurring 3, 5 and 7 days following *Sox9* deletion. Nearly complete suppression of Sox9 expression was already observed by 3 days, concomitant with altered expression of lysozyme, Muc2, and Klf4 in Paneth cells (Figure S8a). In contrast, no evidence of type 2 immune responses (increased numbers of *lamina propria* Gata3$^+$ cells; Figure S8b) or IL13-dependent epithelial remodelling (Retnlβ expression, increased frequency of Dclk1$^+$ tuft cells, increased RegIII expression; Figure S8b and S8c) was observed at this time point. However, by 5 days after initiation of tamoxifen treatment, Gata3$^+$ immune cell numbers were increased but no evidence of epithelial remodelling was detected (Figure S8b). Finally, after 7 days, the elevated numbers of Gata3$^+$ immune cells in the *lamina propria* were associated with epithelial remodelling, as assessed by changes in Retnlβ, Dclk1 and RegIII expression (Figure S8b and S8c).

Altogether, our study demonstrates that Sox9-deficient Paneth cells cause chronic type 2 inflammation and the establishment of dysbiosis via a three step pathway requiring a crosstalk between Paneth and tuft cells (Figure 7and S9). Moreover, our findings imply a yet unidentified but critical homeostatic function of Paneth cells in controlling succinate-producing microbiota species to prevent the inappropriate activation of tuft cells in the absence of a parasite infection, and subsequent deleterious dysbiosis. Finally, our findings that inhibition of either SucnR1 signalling on tuft cells or IL4R/IL13R signalling on target epithelial cells disrupt the feedback to Paneth cells with a subsequent attenuation of dysbiosis, identify pathways that may be therapeutically targeted in patients with dysbiosis.

Discussion

Many genetic and environmental factors can impair Paneth cell function, resulting in dysbiosis and increased susceptibility to chronic diseases (14, 16, 15, 7, 17, 19). To assess the impact of

dysfunctional Paneth cells in adult intestinal physiopathology, we generated an inducible allele for *Sox9* deletion. Although we and others previously reported an absence of Paneth cells in mice in which *Sox9* deletion in the gut epithelium occurred during embryo development (12, 13), induction of its deletion in adult mice did not impair Paneth cell lineage specification but these cells had an altered phenotype. This suggests additional Sox9 roles during embryonic development that specify the Paneth cell lineage. In our adult model, morphological defects in Paneth cells are reminiscent of those present in Paneth cells from IBD patients (14, 15) and obese subjects (16), two conditions strongly linked to dysbiosis. Our data confirm the central role of Sox9 specifically in Paneth cells since, 1- defects in Paneth cells, as well as type 2 immune responses, are absent in *Sox9*$^{LoxP/LoxP}$*;P450a1-Cre* mice, where Sox9 is deleted in all intestinal epithelial cells except Paneth cells, and, 2- the specific deletion of lysozyme in Paneth cells in the gut is sufficient to cause a type 2 immune response (19). Taking advantage of this model to assess the underlying mechanisms responsible for dysbiosis initiation and inflammation induced by Paneth cell defects, we investigated the potential involvement of tuft cells, sentinel cells in the intestinal epithelium that are capable of integrating host-microorganism interactions to regulate mucosal immunity. The findings reported here now establish sentinel tuft cells as central contributors to dysbiosis and chronic inflammation following primary Paneth cell defects. Notably, on its own, Paneth cell dysfunction has only limited pathological consequences. We thus identify a novel Paneth-tuft cell crosstalk that is critical to promote gut dysbiosis.

Tuft cells can be activated by various metabolites. In the context of parasite infection, where tuft cells are indispensable in the initiation of anti-helminthic and anti-protozoan immunity (20–22), the *Tritrichomonas* protist-derived metabolite succinate is able to activate tuft cells and trigger a type 2 immune response as well as adaptative small-intestinal remodelling (25, 26). Moreover, extracts of the parasitic helminth *Trichinella spiralis* can activate tuft cells through Tas2r bitter-taste receptors to initiate type 2 immunity (27). Recently, binding of the N-undecanoylglycine bacterial metabolite to the vomeronasal Vmn2r26 receptor on the tuft-2 tuft cell subset was shown to facilitate bacterial eradication through prostaglandin-D2 signaling and increased mucus secretion (23). However, potential tuft cell function in the context of endogenous microbiota had not been evaluated. Our data indicate that tuft cells activated following Paneth cell dysfunction play a critical role in promoting microbiota remodelling and subsequent inflammation. Mechanistically, this is likely mediated by down-regulation of Paneth cell-expressed antibacterial lectins *RegIII*β and *RegIII*γ, previously recognized for their roles in regulating microbial populations (43) and their involvement in dysbiosis (44, 45). Thus, initial Paneth cell defects, with limited impact on microbiota composition, activate tuft cells. Activated tuft cells, in turn, trigger type 2 inflammation, which causes additional Paneth cell alterations and increased trans-epithelial permeability, possibly through alteration of Claudin adhesion proteins expression as already reported in the context of exposure

to different inflammatory cytokines (46). The mechanisms underlying the latter remain unclear but likely involve the microbiota and/or the effects of type 2 cytokines on epithelial cells as increased permeability is absent in both antibiotic-treated and Il4rα-deficient mice. Based on these data, it is interesting to speculate that tuft cells may play a role in the pathogenesis and pathophysiology of numerous diseases associated with Paneth cell defects, caused by either environmental stressors and/ or genetic predisposition.

Our study highlights a central role for microbe-derived succinate in the activation of tuft cells following Paneth cell alterations. Luminal succinate was previously reported to activate tuft cells in the context of parasitic infection by *Tritrichomonas* (25, 26), or after artificial perturbations in the microbiota composition (24). Such activation requires the Sucnr1 succinate receptor, which, in the intestinal epithelium, is specifically expressed by tuft cells. Interestingly, obese and Crohn's disease patients, both with altered Paneth cells, have a dysbiotic microbiota with increased capacity to produce succinate (47, 48). In the mammalian gut, succinate is mainly produced by bacteria belonging to the *Bacteroidetes* phylum and monocolonization of germ-free mice with *Bacteroides vulgatus* (recently reclassified as Phocaeicola vulgatus), a species known to be associated with intestinal inflammation when present in high concentration (49), is sufficient to increase caecal succinate levels (50). Importantly, we found that *Bacteroides vulgatus* species were enriched in the caecum of dysbiotic *Sox9$^{LoxP/LoxP}$;Villin-Cre^{ERT2}* mice, in which metagenomic analyses revealed increased succinate production potential. Furthermore, using compound *Sox9$^{LoxP/LoxP}$;Villin-Cre^{ERT2};Sucnr1$^{-/-}$* mice with altered Paneth cells, we demonstrated a central role of succinate in activating tuft cells. While increased luminal succinate concentrations are essential for the induction of tuft cell-triggered immune responses against parasite infections, our results suggest that excessive representation of succinate-producing endogenous bacterial species can have a detrimental impact. Consequently, our data highlight a novel key role of Paneth cells in controlling endogenous succinate-producing bacteria to avoid illegitimate tuft cell activation. We have thus identified a previously unsuspected "Paneth cell-tuft cell" crosstalk, regulated by the luminal microorganism composition, to control gut mucosal immunity. While this crosstalk is critical in preventing tuft cell activation in the absence of parasite infections, it may also be involved in pathophysiological situations. For instance, Paneth cell alterations have been observed following mouse infection with the *Nippostrongylus brasiliensis* helminth, with concomitant down-regulation of RegIIIγ and Lysozymes 1 and 2, and these alterations were dependent on IL13- and Stat6-signalling (51). In addition, helminth infections modulate bacterial microbiota composition and, conversely, microbiota impact parasitic colonization (52). Therefore, it is plausible that following parasitic infection, microbiota changes and subsequent Paneth cell alterations may lead to an increase in succinate-producing bacterial species to reinforce type 2 immune responses, promoting helminth expulsion.

Tuft cell signaling downstream of SucnR1 activation has, thus far, been found to depend on Trpm5, following parasite infections or treatment with succinate (24, 25), although some elements of the type 2 immune response were still present in *Trpm5*-deficient mice treated with succinate in drinking water (26). In our study, it is striking that Trpm5 was dispensable for the SucnR1-dependent tuft cell activation in response to endogenous microbiota, suggesting that specific triggers may activate distinct tuft cell signaling pathways, potentially resulting in differential impacts on mucosal immunity.

In conclusion, our data support the host+microbiota ecosystem model, also called a holobiont (1), wherein there is a bidirectional interaction between microbial composition and the host inflammation status. Our study reveals a new component, a Paneth cell-tuft cell crosstalk, opening perspectives for combinatorial therapies targeting both host and microbiota for a more effective management of dysbiosis-associated chronic diseases.

Materials and Methods

Animal strains

All animal studies were approved by the Ministère de l'Enseignement Supérieur, de la Recherche et de l'Innovation (APAFIS#10413-2017062817274261 v2). Animals were housed in an SPF animal facility and male and female mice were analysed between 10 and 16 weeks of age. All mice were on a C57BL/6 genetic background (except those containing the *IL4Ra*$^{-/-}$ allele, which are on a mixed genetic background). The *Sox9*$^{LoxP/LoxP}$*;Villin-Cre*^{ERT2} conditional mouse model was generated by crossing *Sox9*$^{LoxP/LoxP}$ mice (53) with *Villin-Cre*^{ERT2} mice (54). The *Pou2f3*-deficient model has been described previously (55). The *Pou2f3*$^{-/-}$ mice have been crossed with *Sox9*$^{LoxP/LoxP}$*;Villin-Cre*^{ERT2} mice to generate the *Sox9*$^{LoxP/LoxP}$*;Villin-Cre*^{ERT2}*;Pou2f3*$^{-/-}$ mouse model. *Sox9*$^{LoxP/LoxP}$*;Villin-Cre*^{ERT2} mice were also crossed with *IL4Ra*$^{-/-}$ mice kindly provided by J. Allen or *Trpm5*$^{-/-}$ mice from Jackson Laboratory (56) to establish *Sox9*$^{LoxP/LoxP}$*;Villin-Cre*^{ERT2}*;IL4Ra*$^{-/-}$ and *Sox9*$^{LoxP/LoxP}$*;Villin-Cre*^{ERT2}*;Trpm5*$^{-/-}$ models. *SucnR1*$^{-/-}$ mice were from the Cyagen company and were crossed with *Sox9*$^{LoxP/LoxP}$*;Villin-Cre*^{ERT2} mice to generate the *Sox9*$^{LoxP/LoxP}$*;Villin-Cre*^{ERT2}*;SucnR1*$^{-/-}$ mouse model. All mouse genotypes were obtained by breeding double heterozygous mice, and analysis were performed using littermates. Cre recombinase activity was induced by tamoxifen (Sigma-Aldrich), administrated by oral gavage at daily single dose of 1 mg during 5 days. The *Sox9* $^{LoxP/LoxP}$*;P450a1-Cre* mouse model was established by crossing *Sox9*$^{LoxP/LoxP}$ mice with *P450a1-Cre* mice provided by Douglas Winton (57). Beta-naphthoflavone (βNF, MP Biomedicals) was administered by oral gavage at daily single dose of 2 mg during 5 days as described in (29), to induce p450 responsive element-controlled Cre expression.

RNA extraction and qPCR

Total RNA was extracted from snap-frozen intestinal tissues using TRIzol reagent (Life Technologies) and qPCR was performed using LightCycler 480 SYBR Green I Master (Roche Diagnostics) as previously described (58). Primer sets used for each gene analysed are presented in Table S2. Detailed protocols and information are available in the **Supplementary Materials**.

Transmission electron microscopy

Sample preparation was performed as previously described (59). Detailed protocols and information are available in the **Supplementary Materials**.

Intestinal permeability measurement using FITC-dextran

Paracellular permeability was assessed by measuring the passage of 4kDa FITC-dextran from intestinal lumen into systemic circulation, as previously described (60). Detailed protocols and information are available in the **Supplementary Materials**.

Fluorescent and bright-field immunohistochemistry on paraffin-embedded tissue

Immunohistochemistry analyses were performed as previously reported (20). Detailed protocols and information are available in the **Supplementary Materials**.

Fecal bacterial DNA isolation and 16S rRNA sequencing

Microbial communities profiling was performed by GenoScreen (Lille, France). 16S rDNA-amplicon library was prepared using a 16S primer pair that encompasses a 463 pb targeting the V3-V4 region, using a protocol developed by GenoScreen and named Metabiote®. Detailed protocols and information are available in the **Supplementary Materials**.

Caecal DNA extraction and high throughput metagenomic sequencing

DNA extraction was performed following IHMS SOP 07 V2 for each sample, as previously described (61). Briefly, samples underwent a thermal, chemical and mechanical lysis and operations to eliminate cell debris, proteins, aromatic compounds and RNA. Alcoholic precipitation of DNA salts was performed before cleaning and DNA pellet was reconstituted in TE buffer. Fluorometric Quantitation using Qubit (ThermoFisher Scientific) and FilterMax (Molecular devices) were used to assess the quantity of DNA and Fragment Analyzer 1.0 (Agilent Technologies) was used to assess DNA quality. 3 µg of high molecular weight DNA (>10 kbp) was sheared into fragments of approximately 150 bp using an ultrasonicator (Covaris, Woburn, US) and DNA fragment library construction was performed using the Ion Plus Fragment Library and Ion Xpress Barcode Adaptaters Kits (ThermoFisher Scientific). Purified and amplified DNA fragment libraries were sequenced using the Ion Proton Sequencer (ThermoFisher Scientific), with a minimum of 20 million high-quality reads generated per library. Detailed protocols and information are available in the **Supplementary Materials**.

Organoid culture

Organoid cultures were established from *Sox9*$^{LoxP/LoxP}$ and *Sox9*$^{LoxP/LoxP}$*;Villin-Cre*^{ERT2} intestinal crypts as previously described (62). Detailed protocols and information are available in the **Supplementary Materials**.

Statistical analysis

Statistical analysis was performed using the software GraphPad Prism. For gene expression and intestinal permeability measurements, sample (*n*) was defined as the number of mice used in the experiments, and exact Mann-Whitney U test or Kruskal-wallis test were used to calculate the P value. For histological data quantification, sample (*n*) was defined as the number of cells per crypt-villus unit, and 50 crypt-villus axes were counted per tissue section from at least 3 mice from each genotype. Since normal distribution was tested and was very rarely reached, exact Mann-Whitney U test or Kruskal-wallis test were used to calculate the P value. Results are shown as histograms representing means and standard error of the means (SEM) for each genotype, or as box plot depicting numerical data through their medians and the variability through the minimal to maximal values. No statistical methods were used to predetermine sample size, the experiments were not randomized and the investigators were not blinded during experiments and data assessment. Experiments were replicated at least twice (qPCR, immunohistochemistry, electron microscopy)

except for ethical reasons (intestinal permeability measurements) or due to the cost of the experiments (microbiota sequencing).

Acknowledgments

We acknowledge M. Belkahla, A. Deborgher and C. Joséphine for technical inputs, J. Allen for sharing the IL4r KO mouse line, the RAM-iExplore, RAM-PCEA animal facilities and Luc Forichon for maintenance of mouse colonies, Muriel Asari for iconography, Daniel Fisher and the Jay team for proofreading their critical reading of the manuscript, and the Réseau d'Histologie Expérimentale de Montpellier (RHEM) and the Montpellier RIO Imaging (MRI) facilities. **Funding**: This work was supported by Agence Nationale de la Recherche (ANR-14-CE14-0025-01 and ANR-17-CE15-0016-01 to P.J. and N.T.), Institut National du Cancer (INCa 2014-174 to P.J. and INCA_2018-158 to P.J. and N.T.), SIRIC Montpellier Cancer (grant INCa_Inserm_DGOS_12553 to P.J), the PJ team is "Equipe Labellisée Ligue contre le Cancer"; S.S. was supported by an Inserm-Région Languedoc-Roussillon Fellowship and Ligue Nationale contre le Cancer, J.N. was supported by the Labex EpiGenMed (an "Investissements d'avenir" program ANR-10-LABX-12-01) and Fondation pour la Recherche Médicale (FDT201805005851). Additional funding was from the Metagenopolis grant ANR-11-DPBS-0001.

Data and materials availability: Shotgun metagenomic data are fully available under BioProject ID: PRJEB40719 for shotgun metagenomic data and PRJNA944985 for 16S rRNA sequencing data (http://www.ncbi.nlm.nih.gov/bioproject/944985).

References

1. P. Kundu, E. Blacher, E. Elinav, S. Pettersson, Our Gut Microbiome: The Evolving Inner Self. *Cell* **171**, 1481–1493 (2017).

2. P. J. Turnbaugh, *et al.*, An obesity-associated gut microbiome with increased capacity for energy harvest. *Nature* **444**, 1027–1031 (2006).

3. J. Ni, G. D. Wu, L. Albenberg, V. T. Tomov, Gut microbiota and IBD: causation or correlation? *Nat Rev Gastroenterol Hepatol* **14**, 573–584 (2017).

4. E. Järbrink-Sehgal, A. Andreasson, The gut microbiota and mental health in adults. *Current Opinion in Neurobiology* **62**, 102–114 (2020).

5. C. R. Settanni, G. Ianiro, S. Bibbò, G. Cammarota, A. Gasbarrini, Gut microbiota alteration and modulation in psychiatric disorders: Current evidence on fecal microbiota transplantation. *Progress in Neuro-Psychopharmacology and Biological Psychiatry* **109**, 110258 (2021).

6. R. N. Carmody, *et al.*, Diet dominates host genotype in shaping the murine gut microbiota. *Cell Host Microbe* **17**, 72–84 (2015).

7. Liu, *et al.*, Paneth cell defects in Crohn's disease patients promote dysbiosis. *JCI Insight* **1** (2016).

8. N. H. Salzman, D. Ghosh, K. M. Huttner, Y. Paterson, C. L. Bevins, Protection against enteric salmonellosis in transgenic mice expressing a human intestinal defensin. *Nature* **422**, 522–526 (2003).

9. S. Vaishnava, C. L. Behrendt, A. S. Ismail, L. Eckmann, L. V. Hooper, Paneth cells directly sense gut commensals and maintain homeostasis at the intestinal host-microbial interface. *Proc. Natl. Acad. Sci. U.S.A.* **105**, 20858–20863 (2008).

10. J. H. van Es, *et al.*, Wnt signalling induces maturation of Paneth cells in intestinal crypts. *Nat Cell Biol* **7**, 381–6 (2005).

11. P. Blache, *et al.*, SOX9 is an intestine crypt transcription factor, is regulated by the Wnt pathway, and represses the CDX2 and MUC2 genes. *J Cell Biol* **166**, 37–47 (2004).

12. P. Bastide, *et al.*, Sox9 regulates cell proliferation and is required for Paneth cell differentiation in the intestinal epithelium. *J Cell Biol* **178**, 635–648 (2007).

13. Y. Mori-Akiyama, H. Akiyama, D. H. Rowitch, B. De Crombrugghe, Sox9 is required for determination of the chondrogenic cell lineage in the cranial neural crest. *Proc Natl Acad Sci U S A* **100**, 9360–5 (2003).

14. K. Cadwell, *et al.*, A key role for autophagy and the autophagy gene Atg16l1 in mouse and human intestinal Paneth cells. *Nature* **456**, 259–263 (2008).

15. K. L. VanDussen, *et al.*, Genetic Variants Synthesize to Produce Paneth Cell Phenotypes That Define Subtypes of Crohn's Disease. *Gastroenterology* **146**, 200–209 (2014).

16. C. M. Hodin, *et al.*, Reduced Paneth cell antimicrobial protein levels correlate with activation of the unfolded protein response in the gut of obese individuals. *The Journal of Pathology* **225**, 276–284 (2011).

17. X. Guo, *et al.*, High Fat Diet Alters Gut Microbiota and the Expression of Paneth Cell-Antimicrobial Peptides Preceding Changes of Circulating Inflammatory Cytokines. *Mediators Inflamm* **2017**, 9474896 (2017).

18. J. Wehkamp, E. F. Stange, Paneth's disease. *Journal of Crohn's and Colitis* **4**, 523–531 (2010).

19. S. Yu, *et al.*, Paneth Cell-Derived Lysozyme Defines the Composition of Mucolytic Microbiota and the Inflammatory Tone of the Intestine. *Immunity* **53**, 398-416.e8 (2020).

20. F. Gerbe, *et al.*, Intestinal epithelial tuft cells initiate type 2 mucosal immunity to helminth parasites. *Nature* **529**, 226–230 (2016).

21. M. R. Howitt, *et al.*, Tuft cells, taste-chemosensory cells, orchestrate parasite type 2 immunity in the gut. *Science* **351**, 1329–1333 (2016).

22. J. von Moltke, M. Ji, H.-E. Liang, R. M. Locksley, Tuft-cell-derived IL-25 regulates an intestinal ILC2–epithelial response circuit. *Nature* **529**, 221–225 (2016).

23. Z. Xiong, *et al.*, Intestinal Tuft-2 cells exert antimicrobial immunity via sensing bacterial metabolite N-undecanoylglycine. *Immunity* **55**, 686-700.e7 (2022).

24. W. Lei, *et al.*, Activation of intestinal tuft cell-expressed Sucnr1 triggers type 2 immunity in the mouse small intestine. *PNAS* **115**, 5552–5557 (2018).

25. M. S. Nadjsombati, *et al.*, Detection of Succinate by Intestinal Tuft Cells Triggers a Type 2 Innate Immune Circuit. *Immunity* **49**, 33-41.e7 (2018).

26. C. Schneider, *et al.*, A Metabolite-Triggered Tuft Cell-ILC2 Circuit Drives Small Intestinal Remodeling. *Cell* (2018) https:/doi.org/10.1016/j.cell.2018.05.014 (July 6, 2018).

27. X.-C. Luo, *et al.*, Infection by the parasitic helminth Trichinella spiralis activates a Tas2r-mediated signaling pathway in intestinal tuft cells. *PNAS*, 201812901 (2019).

28. A. Banerjee, *et al.*, Succinate Produced by Intestinal Microbes Promotes Specification of Tuft Cells to Suppress Ileal Inflammation. *Gastroenterology* **159**, 2101-2115.e5 (2020).

29. H. Ireland, C. Houghton, L. Howard, D. J. Winton, Cellular inheritance of a Cre-activated reporter gene to determine Paneth cell longevity in the murine small intestine. *Dev Dyn* **233**, 1332–6 (2005).

30. J. P. Katz, *et al.*, The zinc-finger transcription factor Klf4 is required for terminal differentiation of goblet cells in the colon. *Development* **129**, 2619–2628 (2002).

31. W. D. Troughton, J. S. Trier, Paneth and goblet cell renewal in mouse duodenal crypts. *J Cell Biol* **41**, 251–68 (1969).

32. C. L. Wilson, *et al.*, Regulation of Intestinal α-Defensin Activation by the Metalloproteinase Matrilysin in Innate Host Defense. *Science* **286**, 113–117 (1999).

33. S. Sankaran-Walters, R. Hart, C. Dills, Guardians of the Gut: Enteric Defensins. *Front Microbiol* **8** (2017).

34. A. P. B. Moreira, T. F. S. Texeira, A. B. Ferreira, M. do C. G. Peluzio, R. de C. G. Alfenas, Influence of a high-fat diet on gut microbiota, intestinal permeability and metabolic endotoxaemia. *British Journal of Nutrition* **108**, 801–809 (2012).

35. S. C. Bischoff, *et al.*, Intestinal permeability – a new target for disease prevention and therapy. *BMC Gastroenterol* **14** (2014).

36. N. Thevaranjan, *et al.*, Age-Associated Microbial Dysbiosis Promotes Intestinal Permeability, Systemic Inflammation, and Macrophage Dysfunction. *Cell Host Microbe* **21**, 455-466.e4 (2017).

37. T. Hoyler, *et al.*, The Transcription Factor GATA-3 Controls Cell Fate and Maintenance of Type 2 Innate Lymphoid Cells. *Immunity* **37**, 634–648 (2012).

38. D. Artis, *et al.*, RELMbeta/FIZZ2 is a goblet cell-specific immune-effector molecule in the gastrointestinal tract. *Proc Natl Acad Sci U S A* **101**, 13596–600 (2004).

39. J. F. Urban Jr., *et al.*, IL-13, IL-4Ralpha, and Stat6 are required for the expulsion of the gastrointestinal nematode parasite Nippostrongylus brasiliensis. *Immunity* **8**, 255–64 (1998).

40. F. De Vadder, *et al.*, Microbiota-Produced Succinate Improves Glucose Homeostasis via Intestinal Gluconeogenesis. *Cell Metabolism* **24**, 151–157 (2016).

41. N. Gassler, Paneth cells in intestinal physiology and pathophysiology. *World J Gastrointest Pathophysiol* **8**, 150–160 (2017).

42. M. Barner, M. Mohrs, F. Brombacher, M. Kopf, Differences between IL-4Ra-deficient and IL-4-deficient mice reveal a role for IL-13 in the regulation of Th2 responses (1998).

43. N. H. Salzman, C. L. Bevins, Dysbiosis—A consequence of Paneth cell dysfunction. *Seminars in Immunology* **25**, 334–341 (2013).

44. S. Vaishnava, *et al.*, The Antibacterial Lectin RegIIIγ Promotes the Spatial Segregation of Microbiota and Host in the Intestine. *Science* **334**, 255–258 (2011).

45. L. M. Loonen, *et al.*, REG3γ-deficient mice have altered mucus distribution and increased mucosal inflammatory responses to the microbiota and enteric pathogens in the ileum. *Mucosal Immunology* **7**, 939–947 (2014).

46. S. Prasad, *et al.*, Inflammatory processes have differential effects on claudins 2, 3 and 4 in colonic epithelial cells. *Laboratory Investigation* **85**, 1139–1162 (2005).

47. J. Connors, N. Dawe, J. Van Limbergen, The Role of Succinate in the Regulation of Intestinal Inflammation. *Nutrients* **11**, 25 (2018).

48. C. Serena, *et al.*, Elevated circulating levels of succinate in human obesity are linked to specific gut microbiota. *ISME J* **12**, 1642–1657 (2018).

49. S. M. Bloom, *et al.*, Commensal Bacteroides Species Induce Colitis in Host-Genotype-Specific Fashion in a Mouse Model of Inflammatory Bowel Disease. *Cell Host & Microbe* **9**, 390–403 (2011).

50. H. Setoyama, A. Imaoka, H. Ishikawa, Y. Umesaki, Prevention of gut inflammation by Bifidobacterium in dextran sulfate-treated gnotobiotic mice associated with Bacteroides strains isolated from ulcerative colitis patients. *Microbes and Infection* **5**, 115–122 (2003).

51. W. F. Fricke, *et al.*, Type 2 immunity-dependent reduction of segmented filamentous bacteria in mice infected with the helminthic parasite Nippostrongylus brasiliensis. *Microbiome* **3**, 40 (2015).

52. L. A. Reynolds, B. B. Finlay, R. M. Maizels, Cohabitation in the Intestine: Interactions among Helminth Parasites, Bacterial Microbiota, and Host Immunity. *The Journal of Immunology* **195**, 4059–4066 (2015).

53. R. Kist, H. Schrewe, R. Balling, G. Scherer, Conditional inactivation ofSox9: A mouse model for campomelic dysplasia. *genesis* **32**, 121–123 (2002).

54. F. El Marjou, *et al.*, Tissue-specific and inducible Cre-mediated recombination in the gut epithelium. *genesis* **39**, 186–193 (2004).

55. I. Matsumoto, M. Ohmoto, M. Narukawa, Y. Yoshihara, K. Abe, Skn-1a (Pou2f3) specifies taste receptor cell lineage. *Nat Neurosci* **14**, 685–687 (2011).

56. Y. Zhang, *et al.*, Coding of Sweet, Bitter, and Umami Tastes: Different Receptor Cells Sharing Similar Signaling Pathways. 9 (2003).

57. H. Ireland, *et al.*, Inducible cre-mediated control of gene expression in the murine gastrointestinal tract: effect of loss of β-catenin. *Gastroenterology* **126**, 1236–1246 (2004).

58. M. Bruschi, *et al.*, Loss of Apc Rapidly Impairs DNA Methylation Programs and Cell Fate Decisions in Lgr5+ Intestinal Stem Cells. *Cancer Research* **80**, 2101–2113 (2020).

59. N. Chauvet, *et al.*, Complementary actions of dopamine D2 receptor agonist and anti-vegf therapy on tumoral vessel normalization in a transgenic mouse model. *International Journal of Cancer* **140**, 2150–2161 (2017).

60. J. Karhausen, *et al.*, Epithelial hypoxia-inducible factor-1 is protective in murine experimental colitis. *J. Clin. Invest.* **114**, 1098–1106 (2004).

61. V. Meslier, *et al.*, Mediterranean diet intervention in overweight and obese subjects lowers plasma cholesterol and causes changes in the gut microbiome and metabolome independently of energy intake. *Gut* **69**, 1258–1268 (2020).

62. T. Sato, *et al.*, Single Lgr5 stem cells build crypt-villus structures in vitro without a mesenchymal niche. *Nature* **459**, 262–265 (2009).

Figure legends

Figure 1. Maintenance of intestinal Paneth cell terminal differentiation requires the Sox9 transcription factor

a, Representative immunofluorescence co-staining of Lyz and β-catenin showing the presence of Lyz^+ Paneth cells 2 weeks after tamoxifen-induced *Sox9* deletion in adult epithelial cells (*Sox9$^{LoxP/LoxP}$;Villin-Cre^{ERT2}* mice). Delocalized Paneth cells are indicated with a white arrowhead. Images are representative of 3 mice per genotype, 3 independent experiments.

b, Representative immunofluorescence co-staining of Sox9, Lyz and β-catenin showing deletion of *Sox9* in stem cells, Paneth cells and progenitors in *Sox9$^{LoxP/LoxP}$;Villin-Cre^{ERT2}* mice (white arrowhead) 2 weeks following tamoxifen treatment. Sox9 expression is maintained in Paneth cells (yellow arrowhead) in *Sox9$^{LoxP/LoxP}$;P450a1-Cre* mice (3 mice per genotype), 3 independent experiments.

c, Electron micrographs from small intestine highlighting physiological secretory granules in Paneth cells (arrows) in control *Sox9$^{LoxP/LoxP}$ mice* (*n* = 4) whereas secretory granules in *Sox9*-deficient Paneth cells from *Sox9$^{LoxP/LoxP}$;Villin-Cre^{ERT2}* mice (*n* = 5, >30 days post tamoxifen treatment) are less electron-dense and exhibit heterogeneity in size, shape and number. In contrast, secretory granules exhibit normal structure in mice with a *Sox9* deletion in all epithelial cells except for Paneth cells (*Sox9$^{LoxP/LoxP}$;P450a1-Cre*; *n* = 2, 1 week post-βNF treatment).

d, Representative immunofluorescence co-staining of Muc2, Lyz and β-catenin in *Sox9$^{LoxP/LoxP}$* and *Sox9$^{LoxP/LoxP}$;Villin-Cre^{ERT2}* mice (n = 3 per genotype, 2 weeks following tamoxifen treatment). Muc2 expression in Paneth cells was only detected following *Sox9* deletion in all epithelial cells (white arrowheads).

e, Expression of Paneth cell markers in *Sox9$^{LoxP/LoxP}$* and *Sox9$^{LoxP/LoxP}$;Villin-Cre^{ERT2}* small intestine was evaluated by RT-qPCR analysis in *Sox9$^{LoxP/LoxP}$;Villin-Cre^{ERT2}* and *Sox9$^{LoxP/LoxP}$* mice (n = 4 and n = 5, respectively; 2 weeks after tamoxifen treatment). Data are shown as a ratio of expression relative to *Sox9$^{LoxP/LoxP}$* mice.

Scale bars: 20 μm (**a, b, d**), 2 μm (**c**).

(**e**) Mann-Whitney U test; **P*<0.05; ***P*<0.01.

See also Figure S1

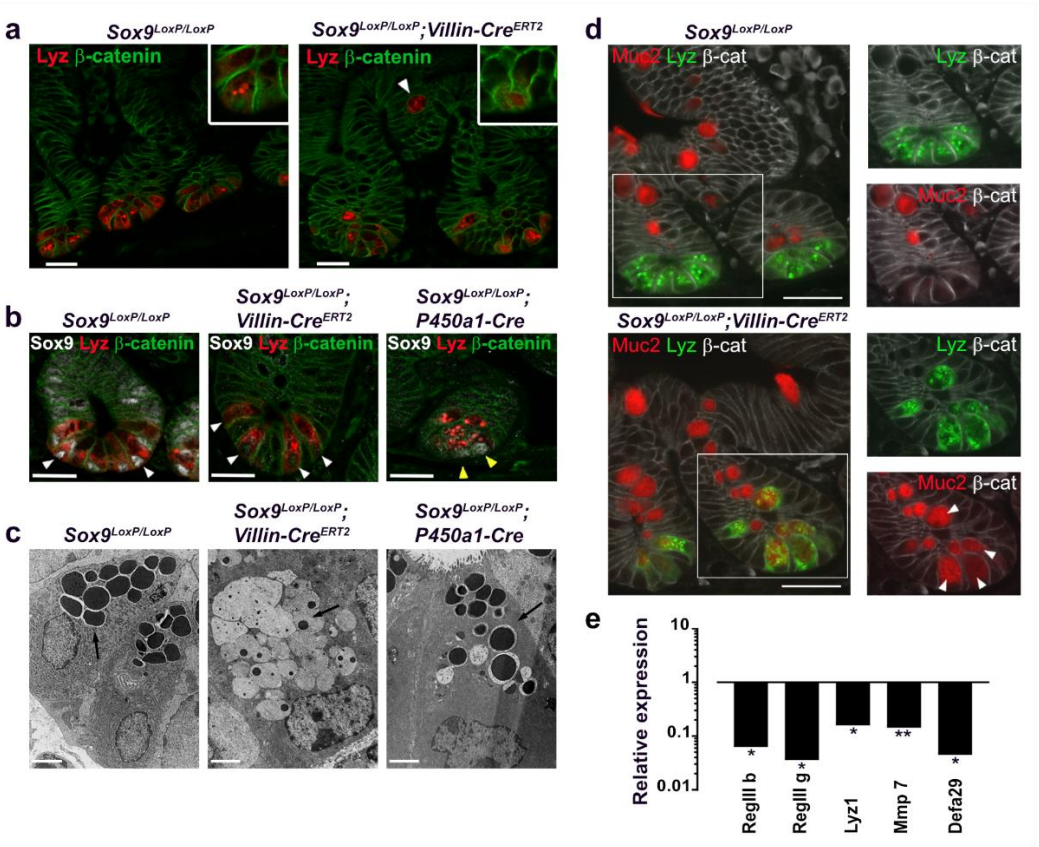
a
Sox9LoxP/LoxP
Lyz β-catenin
Sox9LoxP/LoxP;Villin-CreERT2
Lyz β-catenin
b
Sox9LoxP/LoxP
Sox9 Lyz β-catenin
Sox9LoxP/LoxP; Villin-CreERT2
Sox9 Lyz β-catenin
Sox9LoxP/LoxP; P450a1-Cre
Sox9 Lyz β-catenin
c
Sox9LoxP/LoxP
Sox9LoxP/LoxP; Villin-CreERT2
Sox9LoxP/LoxP; P450a1-Cre
d
Sox9LoxP/LoxP
Muc2 Lyz β-cat
Lyz β-cat
Muc2 β-cat
Sox9LoxP/LoxP;Villin-CreERT2
Muc2 Lyz β-cat
Lyz β-cat
Muc2 β-cat
e
Relative expression
10
1
0.1
0.01
RegIII b
RegIII g
Lyz1
Mmp 7
Defa29

Figure 2. Alterations of gut microbiota and intestinal barrier are associated with abnormal Paneth cells

a, β diversity in microbial communities from *Sox9*$^{LoxP/LoxP}$ and *Sox9*$^{LoxP/LoxP}$*;Villin-Cre*^{ERT2} mice (*n* = 8 mice per genotype). Unweighted principal component analyses (PCA) of Unifrac Distance after 16S rRNA sequencing of faecal microbial populations are presented.

b, Intestinal permeability, assessed by oral gavage of FITC-dextran, was evaluated in control mice (*Sox9*$^{LoxP/LoxP}$ 2 weeks post tamoxifen treatment, n = 7), following deletion of *Sox9* in all epithelial cells (*Sox9*$^{LoxP/LoxP}$*;Villin-Cre*^{ERT2} mice; 2 weeks post tamoxifen treatment, n = 7) or under conditions where Sox9 expression was maintained in Paneth cells (*Sox9*$^{LoxP/LoxP}$*;P450a1-Cre* mice; 2 weeks post βNF treatment, *n* = 3).

(b) Kruskal-Wallis test with Dunn's post hoc test; NS: Not Significant; **P*<0.05. The line indicates the median, the box marks the 25th and 75th percentiles and the whiskers indicate the minimal to maximum values.

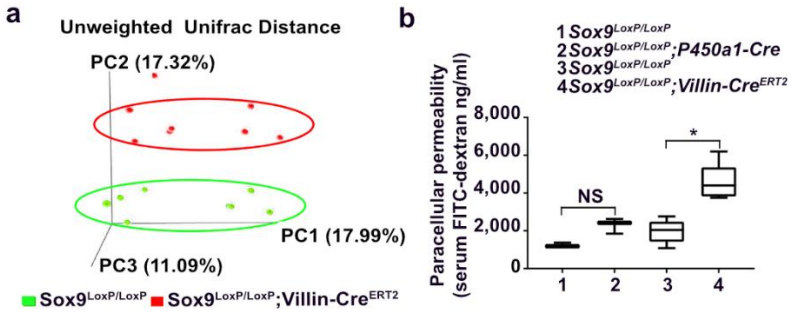

Figure 3. Presence of a type 2 immune response in mice with abnormal Paneth cells

a, Interleukins and transcription factors associated with type 1, 2 and 17 immunity were evaluated in *Sox9*$^{LoxP/LoxP}$ (n = 4) and *Sox9*$^{LoxP/LoxP}$*;Villin-Cre*^{ERT2} (n = 5) small intestine by RT-qPCR analysis. Data are shown as a ratio relative to expression in *Sox9*$^{LoxP/LoxP}$ mice.

b, Representative immunostainings of Mbp, a marker of eosinophilia, and Gata3, a marker of Th2 lymphocytes and ILC2, in Sox9-deficient *lamina propria* in small intestinal epithelium of *Sox9*$^{LoxP/LoxP}$ and *Sox9*$^{LoxP/LoxP}$*;Villin-Cre*^{ERT2} mice. *n* = 3 mice per genotype, sacrificed 2 weeks after tamoxifen treatment.

c, Quantification of MBP and Gata3^{+} cells in *Sox9*$^{LoxP/LoxP}$ and *Sox9*$^{LoxP/LoxP}$*;Villin-Cre*^{ERT2} mice. Cells positive for MBP or Gata3 were counted in *n* = 50 crypt-villus units per mouse (*n* = 3 mice per genotype).

d, Representative immunostainings illustrating tissue remodelling in small intestinal epithelium from *Sox9*$^{LoxP/LoxP}$*;Villin-Cre*^{ERT2} mice. Dclk1 and PAS stainings, respectively, show tuft cell and goblet hyperplasia in Sox9-deficient small intestine. Retnlβ staining reveals the production of Retnlβ molecule by goblet cells, which are co-stained with alcian blue. *n* = 3 mice per genotype, sacrificed 2 weeks after tamoxifen treatment.

e, Quantification of type 2 immune response markers in *Sox9*$^{LoxP/LoxP}$ and *Sox9*$^{LoxP/LoxP}$*;Villin-Cre*^{ERT2} mice. Cells positive for Dclk1, PAS, Retnlβ, Gata3 or Alcian blue were counted in *n* = 50 crypt-villus units per mouse (*n* = 3 mice per genotype). Mice were sacrificed 2 weeks after tamoxifen treatment.

Scale bars: 20 μm (**b, d**).

(a, c and e) Mann-Whitney U test. **P*<0.05; ***P*<0.01; ****P*<0.001 **(a, c, and e)** Data are shown as means ± S.E.M.

See also Figure S2**.**

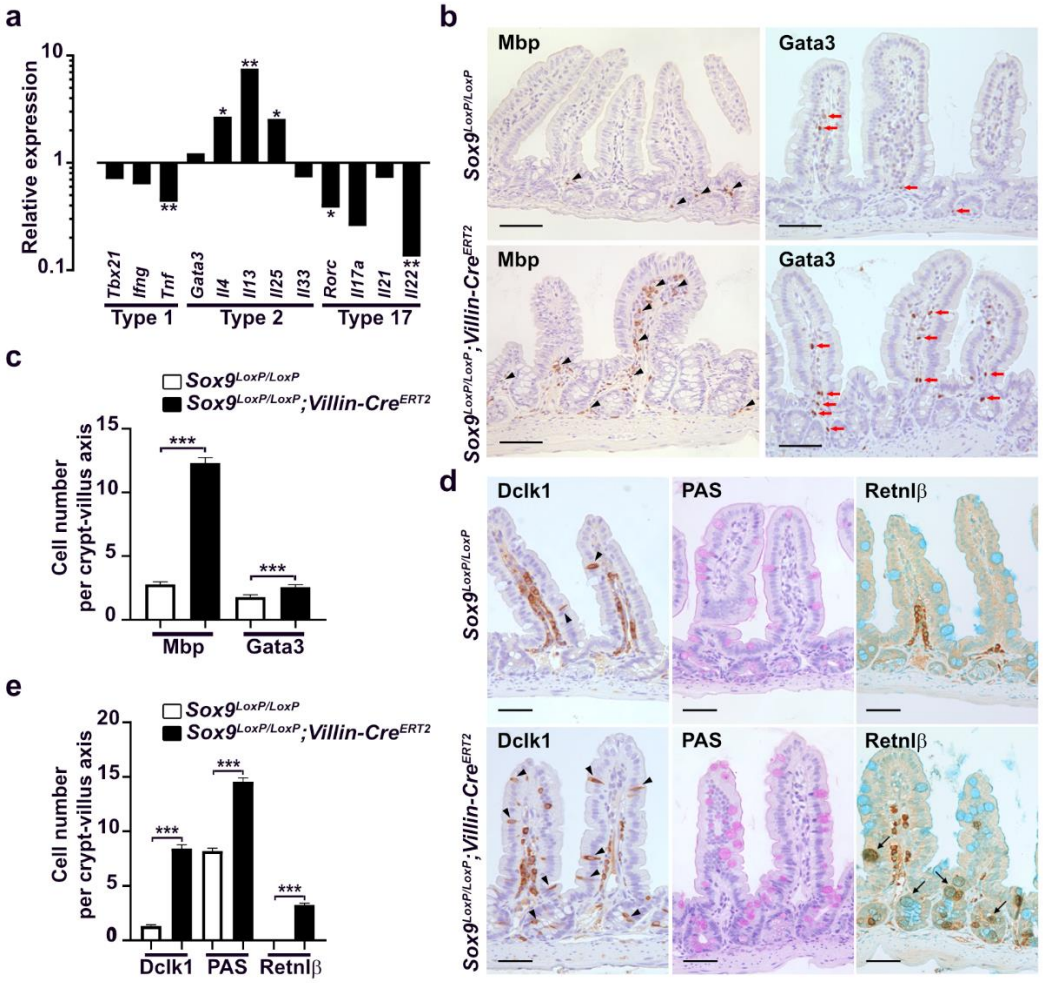
a
Relative expression
10
1
0.1
Tbx21
Ifng
Tnf
Gata3
Il4
Il13
Il25
Il33
Rorc
Il17a
Il21
Il22
Type 1
Type 2
Type 17
b
Mbp
Gata3
Sox9LoxP/LoxP
Sox9LoxP/LoxP;Villin-CreERT2
c
Sox9LoxP/LoxP
Sox9LoxP/LoxP;Villin-CreERT2
Cell number per crypt-villus axis
15
10
5
0
Mbp
Gata3
d
Dclk1
PAS
Retnlβ
e
20
15
10
5
0
Dclk1
PAS
Retnlβ

Figure 4. Presence of tuft cells is required for the development of type 2 immunity and impaired intestinal permeability caused by altered Paneth cells

a, Representative immunofluorescence co-staining of Muc2, Lyz and β-catenin in *Sox9$^{LoxP/LoxP}$;Villin-Cre^{ERT2};Pou2f3$^{-/-}$* mice. Paneth cells lacking Sox9 in a tuft cell-deficient context display an altered differentiation state since Muc2 is present in Paneth cells in *Sox9$^{LoxP/LoxP}$;Villin-Cre^{ERT2}* as well as *Sox9$^{LoxP/LoxP}$;Villin-Cre^{ERT2};Pou2f3$^{-/-}$* mice (white arrowhead), and Lyz staining is diffuse in both genotypes compared to control mice (yellow arrowhead). *n* = 3 mice per genotype, representative of 2 independent experiments. Mice were sacrificed 2 weeks after tamoxifen treatment.

b, Intestinal permeability, assessed by FITC-dextran gavage, remains intact when Sox9 is deleted in a tuft cell-deficient mouse model. FITC-dextran was measured in serum from *Sox9$^{LoxP/LoxP}$;Pou2f3$^{+/+}$* mice (*n* = 4), *Sox9$^{LoxP/LoxP}$;Villin-Cre^{ERT2};Pou2f3$^{+/+}$*mice (*n* = 4), *Sox9$^{LoxP/LoxP}$;Pou2f3$^{-/-}$* mice (*n* = 6) and *Sox9$^{LoxP/LoxP}$;Villin-Cre^{ERT2};Pou2f3$^{-/-}$* mice (*n* = 7). Mice were sacrificed 2 weeks after tamoxifen treatment.

c, The type 2 immune response found in *Sox9$^{LoxP/LoxP}$;Villin-Cre^{ERT2}* mice is abolished in tuft cell-deficient *Sox9$^{LoxP/LoxP}$;Villin-Cre^{ERT2};Pou2f3$^{-/-}$* mice as compared to *Sox9$^{LoxP/LoxP}$;Villin-Cre^{ERT2};Pou2f3$^{+/+}$* mice. Cells positive for Dclk1, Retnlβ, or Gata3 were counted in *n* = 50 crypt-villus units per mouse (*n* = 5-6 mice per genotype).

Scale bars, 20 μm **(a)**.

(b,c) Kruskal-Wallis test with Dunn's post hoc test; NS: Not Significant; **P*<0.05; *****P*<0.0001. **(b)** The line indicates the median, the box marks the 25th and 75th percentiles and the whiskers indicate the minimal to maximum values. **(c)** Data are shown as means ± S.E.M.

See also Figure S4.

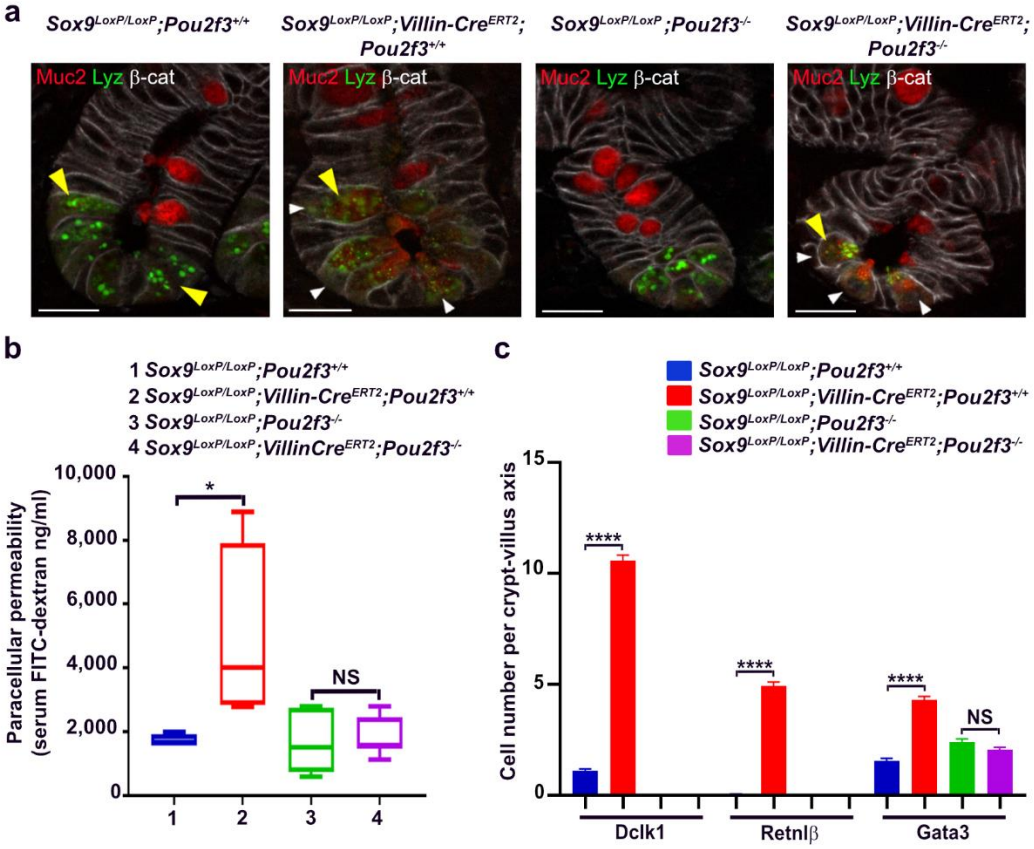
a
Sox9LoxP/LoxP;Pou2f3+/+
Sox9LoxP/LoxP;Villin-CreERT2;Pou2f3+/+
Sox9LoxP/LoxP;Pou2f3-/-
Sox9LoxP/LoxP;Villin-CreERT2;Pou2f3-/-
Muc2 Lyz β-cat
b
1 Sox9LoxP/LoxP;Pou2f3+/+
2 Sox9LoxP/LoxP;Villin-CreERT2;Pou2f3+/+
3 Sox9LoxP/LoxP;Pou2f3-/-
4 Sox9LoxP/LoxP;VillinCreERT2;Pou2f3-/-
Paracellular permeability (serum FITC-dextran ng/ml)
10,000
8,000
6,000
4,000
2,000
0
*
NS
1
2
3
4
c
Sox9LoxP/LoxP;Pou2f3+/+
Sox9LoxP/LoxP;Villin-CreERT2;Pou2f3+/+
Sox9LoxP/LoxP;Pou2f3-/-
Sox9LoxP/LoxP;Villin-CreERT2;Pou2f3-/-
Cell number per crypt-villus axis
15
10
5
0
****
****
****
NS
Dclk1
Retnlβ
Gata3

Figure 5. Increased succinate-producers in the remodeled microbiota of mice with altered Paneth cells lead to tuft cell activation via a succinate-SucnR1 pathway

a, Gene richness in caecum from *Sox9$^{LoxP/LoxP}$;Pou2f3$^{+/+}$*, *Sox9$^{LoxP/LoxP}$;Villin-Cre^{ERT2};Pou2f3$^{+/+}$*, *Sox9$^{LoxP/LoxP}$;Pou2f3$^{-/-}$* and *Sox9$^{LoxP/LoxP}$;Villin-Cre^{ERT2};Pou2f3$^{-/-}$* mice. *n* = 8 mice per genotype. Mice were sacrificed 4 weeks after tamoxifen treatment.

b, Schema of the succinate biosynthetic pathway predominant under anaerobic conditions. The two final steps of the succinate production are shown: (i) the conversion of malate to fumarate by the fumarate hydratase encoded by the *fumABC* genes and (ii) the transformation of fumarate to succinate by the fumarate reductase encoded by the *frdABCD* genes. For each enzymatic reaction, all KO (KEGG Orthologue) alternatives (v1 to v3) found in the KEGG database are shown. Color codes refer to their presence (black) or absence (grey) in the mouse BGI 2.6 million genes catalog.

c, The global completeness of the succinate production pathway is significantly increased in *Sox9$^{LoxP/LoxP}$;Villin-Cre^{ERT2}* mice compared to *Sox9$^{LoxP/LoxP}$* mice. The global completeness for succinate production, i.e. the proportion of KOs detected necessary to produce succinate in each microbial species, was computed for each differentially abundant MSP species found in *Sox9$^{LoxP/LoxP}$* (blue) and *Sox9$^{LoxP/LoxP}$;Villin-Cre^{ERT2}* mice (red).

d, Intestinal permeability, assessed by FITC-dextran gavage, remains intact when *Sox9* is deleted in SucnR1-deficient mice. FITC-dextran was measured in serum from *Sox9$^{LoxP/LoxP}$;SucnR1$^{+/+}$* mice (*n* = 5), *Sox9$^{LoxP/LoxP}$;Villin-Cre^{ERT2};SucnR1$^{+/+}$*mice (*n* = 5), *Sox9$^{LoxP/LoxP}$;SucnR1$^{-/-}$* mice (*n* = 5) and *Sox9$^{LoxP/LoxP}$;Villin-Cre^{ERT2};*SucnR1$^{-/-}$ mice (*n* = 6). Mice were sacrificed 2 weeks after tamoxifen treatment.

e, Type 2 immune response is abolished in absence of SucnR1. Cells positive for Dclk1, Retnlβ, or Gata3 were counted in *n* = 50 crypt-villus units per mouse (*n* = 5-6 mice per genotype).

(a) Unpaired Wilcoxon rank sum test. **(c)** Unpaired Wilcoxon signed rank test, p=0.017. **(d-e)** Kruskal-Wallis test with Dunn's post hoc test; NS: Not Significant; **P*<0.05; ***P*<0.01; ***P<0.001; *****P*<0.0001. **(a, c, d)** The line indicates the median, the box marks the 25th and 75th percentiles and the whiskers indicate the minimal to maximum values. **(e)** Data are shown as means ± S.E.M.

See also Figure S5 and S6.

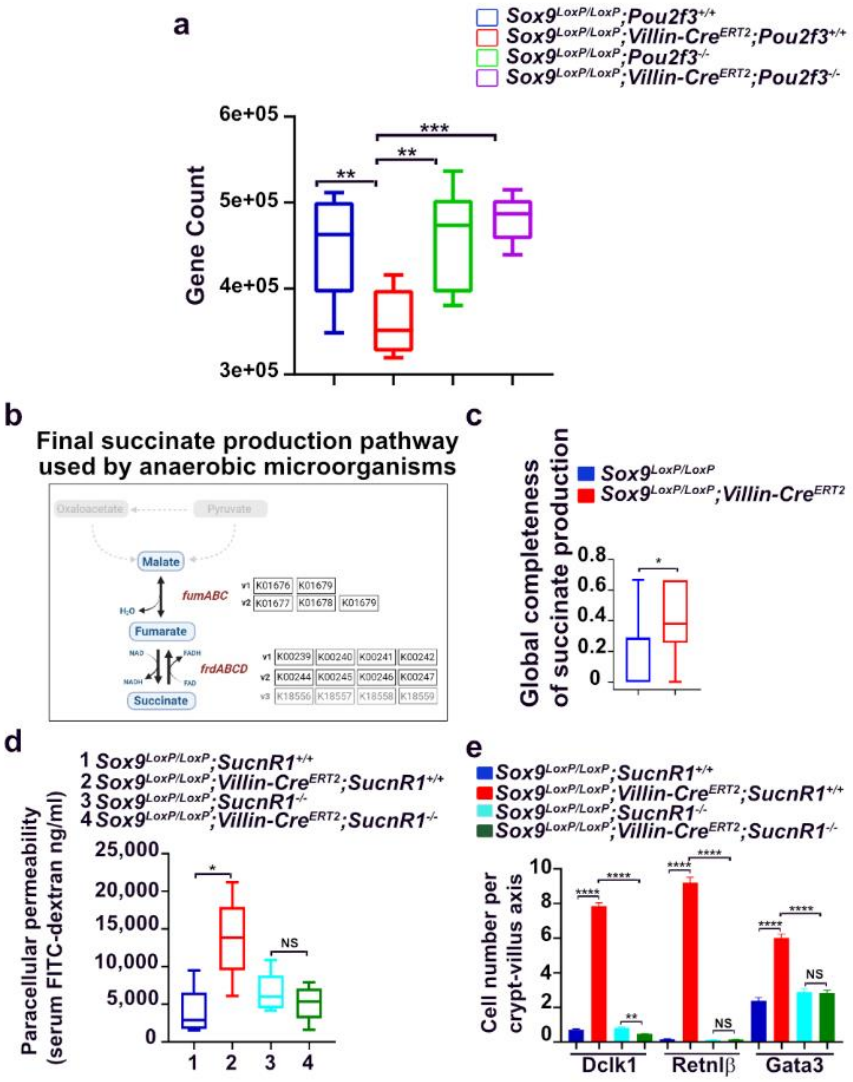
a
Sox9LoxP/LoxP;Pou2f3+/+
Sox9LoxP/LoxP;Villin-CreERT2;Pou2f3+/+
Sox9LoxP/LoxP;Pou2f3-/-
Sox9LoxP/LoxP;Villin-CreERT2;Pou2f3-/-
Gene Count
6e+05
5e+05
4e+05
3e+05
**
**
***
b
Final succinate production pathway used by anaerobic microorganisms
Oxaloacetate
Pyruvate
Malate
fumABC
H2O
Fumarate
NAD
FADH
NADH
FAD
frdABCD
Succinate
v1 K01676 K01679
v2 K01677 K01678 K01679
v1 K00239 K00240 K00241 K00242
v2 K00244 K00245 K00246 K00247
v3 K18556 K18557 K18558 K18559
c
Sox9LoxP/LoxP
Sox9LoxP/LoxP;Villin-CreERT2
Global completeness of succinate production
0.8
0.6
0.4
0.2
0
*
d
1 Sox9LoxP/LoxP;SucnR1+/+
2 Sox9LoxP/LoxP;Villin-CreERT2;SucnR1+/+
3 Sox9LoxP/LoxP;SucnR1-/-
4 Sox9LoxP/LoxP;Villin-CreERT2;SucnR1-/-
Paracellular permeability (serum FITC-dextran ng/ml)
25,000
20,000
15,000
10,000
5,000
0
*
NS
1
2
3
4
e
Sox9LoxP/LoxP;SucnR1+/+
Sox9LoxP/LoxP;Villin-CreERT2;SucnR1+/+
Sox9LoxP/LoxP;SucnR1-/-
Sox9LoxP/LoxP;Villin-CreERT2;SucnR1-/-
Cell number per crypt-villus axis
10
8
6
4
2
0
****
****
**
****
****
NS
****
****
NS
Dclk1
Retnlβ
Gata3

Figure 6. Dysbiosis is dependent on a cross-talk between tuft cells and Paneth cells, via the down-regulation of the antimicrobial RegIII

a, RT-qPCR analysis of antimicrobial peptides *Lyz1*, *Mmp7, Defa29* and *RegIII* in organoids derived from *Sox9*$^{LoxP/LoxP}$ and *Sox9*$^{LoxP/LoxP}$*;Villin-Cre*^{ERT2} small intestine. Organoids were analysed 5 days after 4-OH-tamoxifen treatment (*n*= 2 independent organoid cultures, replicated 3 times).

b, RT-qPCR analysis of antimicrobial peptides *Lyz1*, *Mmp7, Defa29* and *RegIII* in *Sox9*$^{LoxP/LoxP}$*;Villin-Cre*^{ERT2} and *Sox9*$^{LoxP/LoxP}$*;Villin-Cre*^{ERT2}*;Pou2f3*$^{-/-}$ small intestine. *n* = 6-8 mice per genotype. Mice were sacrificed 2 weeks after tamoxifen treatment.

(a) Mann-Whitney U test. **(b)** Kruskal-Wallis test with Dunn's post hoc test; NS: Not Significant; **P*<0.05; ***P*<0.01; ****P*<0.001. The line indicates the median, the box marks the 25th and 75th percentiles and the whiskers indicate the minimal to maximum values.

See also Figure S7.

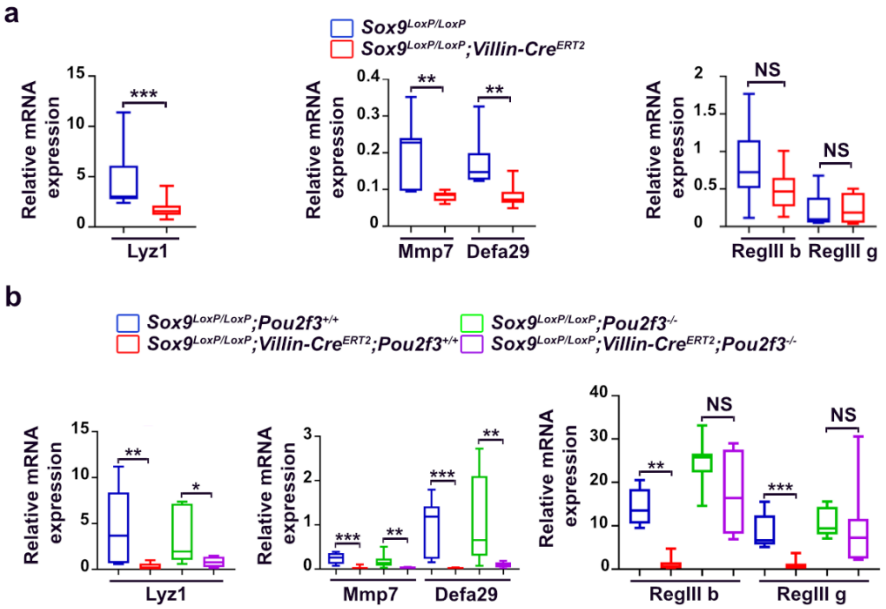

Figure 7. A three-step mechanism for establishment of dysbiosis and inflammation due to the crosstalk between altered Paneth cells and tuft cells through succinate-SucnR1 signalling and type 2 cytokines.

In homeostatic conditions, Paneth cells regulate microbiota composition and the presence of tuft cells is rare. Step 1: In the absence of Sox9, Paneth cells are altered and express normal levels of *RegIII* but lower levels of *Lyz1*, leading to mild alterations in the microbiota and increased succinate production potential. Step 2: Sensing of increased succinate levels by tuft cells, via the SucnR1, results in the initiation of a type 2 immune response. Step 3: Type 2 cytokines cause IL4rα-dependent remodelling of epithelial cells, including ectopic Retnlβ expression in goblet cells, tuft cell lineage amplification, and reduction of *RegIII* levels. This remodelling accentuates the deficiency in microbiota regulation by epithelial cells, eventually causing dysbiosis. As tuft cells cooperate with altered Paneth cells to drive dysbiosis, pharmacological inhibition of tuft cell activity may represent a novel strategy for controlling inflammation and dysbiosis in predisposed patients with altered Paneth cells.

See also Figures S8 and S9.